

Haverford College

## Haverford Scholarship

---

Faculty Publications

Physics

---

2010

### Differential Embedding of the Lorenz Attractor

Daniel J. Cross

*Haverford College*, [dcross@haverford.edu](mailto:dcross@haverford.edu)

Follow this and additional works at: [https://scholarship.haverford.edu/physics\\_facpubs](https://scholarship.haverford.edu/physics_facpubs)

---

#### Repository Citation

"Differential Embedding of the Lorenz Attractor," D. J. Cross and R. Gilmore, *Physical Review E* 81, 066220 (2010).

This Journal Article is brought to you for free and open access by the Physics at Haverford Scholarship. It has been accepted for inclusion in Faculty Publications by an authorized administrator of Haverford Scholarship. For more information, please contact [nmedeiro@haverford.edu](mailto:nmedeiro@haverford.edu).

## Differential embedding of the Lorenz attractor

Daniel J. Cross and R. Gilmore

*Physics Department, Drexel University, Philadelphia, Pennsylvania 19104, USA*

(Received 21 January 2010; published 25 June 2010)

Ideally an embedding of an  $N$ -dimensional dynamical system is  $N$ -dimensional. Ideally, an embedding of a dynamical system with symmetry is symmetric. Ideally, the symmetry of the embedding is the same as the symmetry of the original system. This ideal often cannot be achieved. Differential embeddings of the Lorenz system, which possesses a twofold rotation symmetry, are not ideal. While the differential embedding technique happens to yield an embedding of the Lorenz attractor in three dimensions, it does not yield an embedding of the entire flow. An embedding of the flow requires at least four dimensions. The four dimensional embedding produces a flow restricted to a twisted three dimensional manifold in  $\mathbb{R}^4$ . This inversion symmetric three-manifold cannot be projected into any three dimensional Euclidean subspace without singularities.

DOI: [10.1103/PhysRevE.81.066220](https://doi.org/10.1103/PhysRevE.81.066220)

PACS number(s): 05.45.Xt, 05.45.Ac, 05.45.Gg

### I. INTRODUCTION

The first step in the analysis of data generated by a chaotic dynamical system is the search for an embedding. Often the data set consists of a single long series of observations taken at equally spaced time intervals, or a scalar time series for short. The observed data can be interpreted as the values taken by an observation function on the original phase space, sampled along the observed trajectory. Takens' Theorem [1] guarantees that if the dynamical system that generates the data exists in an  $N$ -dimensional phase space, there is generically an embedding in  $\mathbb{R}^{2N+1}$  that may be constructed from the observed data. While this is adequate for theoretical work, in practice an embedding of lowest possible dimension is preferred. In particular, if the data are generated by an  $N$ -dimensional system, there ought to be an  $N$ -dimensional embedding.

Reconstructions of dynamical systems with symmetry pose a special problem. According to Takens' theorem it is necessary to use a generic observation function for a reconstruction. However, a generic function does not possess a symmetry, and an embedding made using such an observable lacks symmetry. Worse, King, and Stewart [2] showed that an observable with some symmetry can be used for an embedding, but that the embedding typically does not possess the same symmetry as the original dynamical system. This was shown explicitly by Letellier and his colleagues [3] for the Lorenz dynamical system. In particular, they showed that using an observation function that is odd under the twofold rotation symmetry of the Lorenz attractor will result in a dynamical system with inversion rather than rotation symmetry.

The present work was stimulated by the following difficulty. All inequivalent (nonisotopic) representations (embeddings) of the Lorenz system in  $\mathbb{R}^3$  have been identified [4]. A differential embedding of the Lorenz system based on the  $x$  or  $y$  coordinate produces a system not included in this list of inequivalent representations. We sought to determine how this could be possible. The answer is provided below.

We study this problem for embeddings with minimal time delay. In this case, linear combinations of  $k$  adjacent terms in

the time series are good approximations to the signal and its first  $k-1$  derivatives. For this reason, we call embeddings with minimal time delay *differential embeddings*. Embeddings of this type have four attractive features [5]: (i) Each embedding coordinate is the derivative of the previous coordinate ( $X_{i+1}=\dot{X}_i$ ); (ii) Attempts to model the dynamics using the embedding coordinates involve construction of only one unknown source function [5,3], for the last time derivative  $\dot{X}_N=h(X_1, X_2, \dots, X_N)$ ; (iii) An explicit expression for the source function  $h$  may be constructed when the differential equations are known; and (iv) In three dimensions  $N=3$  it is a simple matter to determine the topological organization of all unstable periodic orbits simply by inspection of their projection onto the  $(X_1, X_2)=(X_1, \dot{X}_1)$  subspace. In this projection, all crossings in the upper half plane have sign  $-1$  while all crossings in the lower half plane have sign  $+1$ . The linking number of two periodic orbits is half the number of crossings in the lower half plane minus half the number of crossings in the upper half plane [6,7].

The principal drawback of differential embeddings of scalar time series is the signal to noise problem. As a rough rule of thumb, there is an order of magnitude loss of  $S/N$  ratio for each derivative (or integral) that is taken. A differential embedding of the type  $x \rightarrow (x, \dot{x}, \ddot{x})$  generally suffers two orders of magnitude reduction in this ratio. One way around this problem is to use an integral-differential embedding  $x \rightarrow (\int x, x, \dot{x})$ . In this case the integral and differential each lose about one order of magnitude. The three coordinates remain differentially related. Care must be taken that secular terms be removed from the scalar time series before the integral is taken. The subtle points involved in such embeddings have been described in the first topological analysis of experimental data that was carried out [5]. These points were amplified on in [6,7].

Briefly, in the first topological analysis, the data set under consideration behaved like a relaxation oscillator, with a slow linear change over about half a cycle. The differential embedding  $(x, \dot{x}, \ddot{x})$  collapsed to a straight line, as can be seen in [5]. Spline fits [8] were unable to lift this degeneracy, as indeed no data processing method based on local fitting methods could succeed. A variety of nonlocal methods were

reviewed in this context [6,7]. More recently, newer data processing methods have been developed to treat problems of this type [9].

A differential embedding of the Lorenz system based on the  $x$  coordinate is called the induced Lorenz system. Its relationship to the original Lorenz system will be investigated. Our main result is that these two systems are diffeomorphic, in fact isotopic, in  $\mathbb{R}^4$ , though not in  $\mathbb{R}^3$ .

The organization of this paper is as follows. In Sec. II, we introduce the Lorenz ( $\mathcal{L}$ ) and induced Lorenz ( $\mathcal{L}_i$ ) systems. In Sec. III, we examine in detail the differential mappings constructed from the  $x$  coordinate of  $\mathcal{L}$  and decide when they furnish embeddings. Singularities found to be present in these mappings are analyzed in Sec. IV where they are shown to be consequences of the different symmetries of  $\mathcal{L}$  and  $\mathcal{L}_i$ . This shows that a three-dimensional reconstruction of the Lorenz system with parity symmetry is never an embedding. In Sec. V, we show that  $\mathcal{L}$  and  $\mathcal{L}_i$  are related by a “local reflection” of  $\mathbb{R}^3$  and are in fact isotopic in  $\mathbb{R}^4$ . We extend this analysis in Sec. VI to the bounding tori and branched manifolds of the two systems. In Sec. VII, we generalize the observation in [3] that equivariant embeddings of the Lorenz system are parity symmetric to arbitrary dynamical systems with a twofold symmetry. We also demonstrate how reconstructions with arbitrary twofold symmetry may be recovered from a generic observation function. Finally, we state our conclusions in Sec. VIII.

**II. LORENZ AND INDUCED LORENZ SYSTEMS**

The Lorenz dynamical system  $\mathcal{L}$  is a three dimensional flow defined by the equations

$$\dot{x} = \sigma(y - x) \tag{1a}$$

$$\dot{y} = Rx - y - xz \tag{1b}$$

$$\dot{z} = -bz + xy. \tag{1c}$$

A dynamical system  $\dot{x}=v(x)$  is said to be equivariant under a linear transformation  $M$  if  $M\dot{x}=v(Mx)$ . The Lorenz system is equivariant under the transformation  $R_z(\pi): (x, y, z) \mapsto (-x, -y, z)$ , which is a  $\pi$  rotation about the  $z$  axis. We say that  $\mathcal{L}$  possesses rotation symmetry or is rotationally equivariant.

The Lorenz branched manifold [3,10,11] is shown in Fig. 1. It is rotationally symmetric. A branched manifold (or knot holder or template) of a strange attractor generated by a three dimensional dynamical system is a two-dimensional manifold almost everywhere (it possesses a finite set of zero and one dimensional singular sets called splitting points and branch lines, respectively) which provides a caricature of the original attractor [6]. Specifically, it supports a semiflow obtained by identifying points in the original system that share the same asymptotic future. This is equivalent to collapsing the stable manifolds to points. This identification is called the Birman Williams projection [10,11].

The template shown in Fig. 1 is obtained from the standard “mask” by rotating each of the two lobes of the mask through 90 degrees in opposite directions, and then viewing

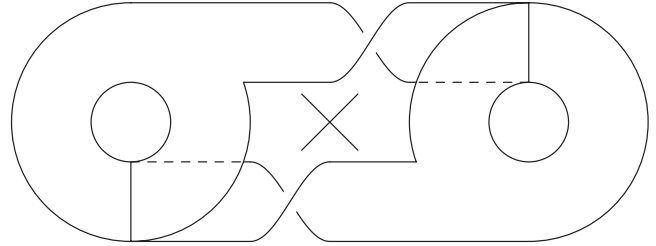


FIG. 1. Template for the Lorenz system  $\mathcal{L}$  with rotation symmetry,  $R_z(\pi)$ . The “ $\times$ ” denotes the central saddle fixed point. The  $x$  and  $y$  directions are in the page, horizontal and vertical respectively. The  $z$  direction is out of the page.

the attractor from above. This procedure preserves the topological organization of the periodic orbits. This transformation is described in more detail in [12,13].

A differential embedding of the Lorenz system based on the  $x$ -coordinate constructs the so-called “induced Lorenz system,”  $\mathcal{L}_i$ . Unlike the original system  $\mathcal{L}$ , the induced system is equivariant under the transformation  $P:(X, Y, Z) \mapsto (-X, -Y, -Z)$ , which is an inversion. We say that  $\mathcal{L}_i$  possesses parity symmetry or is parity equivariant. The induced Lorenz branched manifold [3], which is also parity symmetric, is shown in Fig. 2. The explicit equations describing this embedding are given in the next section.

The induced system passes the usual embedding tests and is regarded as an embedding of the original dynamical system into  $\mathbb{R}^3$  [14]. While this is essentially true on the attracting set, we claim that the mapping giving rise to this “embedding” is in fact not an embedding on any open subset containing the attractor and therefore does not truly represent the entire original flow. We prove this claim in the next section.

**III. DIFFERENTIAL MAPPINGS**

If  $M$  is an  $m$ -dimensional manifold with flow  $\varphi_t$  and  $f: M \rightarrow \mathbb{R}$  a real-valued observation function on  $M$ , then Takens’ theorem [1] states that generically the map  $M \rightarrow \mathbb{R}^{2m+1}$  given by

$$x \mapsto \left\{ f(x), \left. \frac{d}{dt} \right|_0 f[\varphi_t(x)], \dots, \left. \frac{d^{2m}}{dt^{2m}} \right|_0 f[\varphi_t(x)] \right\}, \tag{2}$$

is an embedding. The notation indicates that derivatives are to be evaluated at  $t=0$ . Such a mapping constructed from

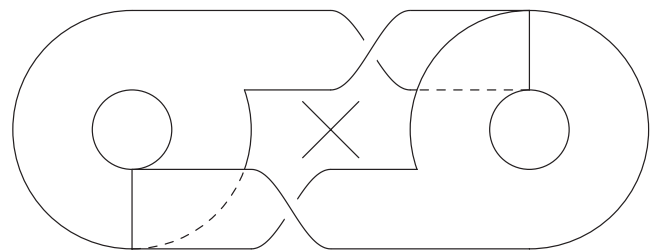


FIG. 2. Template for the induced Lorenz system  $\mathcal{L}_i$  with parity symmetry,  $P$ . The “ $\times$ ” denotes the central saddle fixed point. The coordinate axes are the same as Fig. 1.

successive derivatives of an observation function will be called a differential mapping. When the mapping is an embedding it is called a differential embedding.

Takens' theorem all but guarantees that the differential embedding of  $\mathcal{L}$  constructed from  $x$  and its first six derivatives is an embedding into  $\mathbb{R}^7$ . This leaves open the question of whether an embedding may be found in lower dimensions, which ought to be the case since  $\mathcal{L}$  was originally defined in  $\mathbb{R}^3$ .

Consider  $\mathcal{L}$  with observation function  $f(x)=x$  and define the series of differential mappings

$$F_n(x) = \left( x, \frac{d}{dt}x, \dots, \frac{d^{n-1}}{dt^{n-1}}x \right), \quad (3)$$

for each  $n \geq 3$ . The mapping  $F_3$ , which gives rise to the system  $\mathcal{L}_i$  in  $\mathbb{R}^3$ , is explicitly given by

$$\begin{pmatrix} X \\ Y \\ Z \end{pmatrix} = \begin{pmatrix} x \\ \sigma(y-x) \\ \sigma(R+\sigma-z)x - \sigma(1+\sigma)y \end{pmatrix}. \quad (4)$$

The Jacobian of the transformation is

$$J_3 = \begin{pmatrix} 1 & 0 & 0 \\ -\sigma & \sigma & 0 \\ \sigma(R+\sigma-z) & -\sigma(1+\sigma) & -\sigma x \end{pmatrix}. \quad (5)$$

The Jacobian determinant is  $-\sigma^2x$ , so the mapping is singular on the entire  $yz$  plane. By setting  $x=0$  in  $F_3$  one sees that the mapping collapses lines of constant  $y$  onto points in the  $yz$ -plane, and this is the only set where  $F_3$  fails to be injective. This demonstrates that  $F_3$  is not a diffeomorphism on any open set intersecting the  $yz$  plane ( $x=0$ ). Since the attractor cuts this plane, we conclude that  $F_3$  fails to be a diffeomorphism on any neighborhood containing the attractor.

The existence of these singularities has been known [3,15–18]. In these references, the singularities are interpreted as obstructions to an observation function well-sampling an attractor, a property called observability. However, since the set of singularities has measure zero it has been tacitly assumed that they do not affect whether or not one actually obtains an embedding of the phase space. In other words, obtaining an embedding of the attractor is distinct from and less restrictive than obtaining an embedding of the entire phase space. A three-dimensional differential embedding of the Lorenz system based on the  $x$  coordinate accomplishes the former task, but not the latter. This is why the induced Lorenz system does not appear on the list of inequivalent representations of the Lorenz system—in  $\mathbb{R}^3$  it is not a representation at all.

It is straightforward to derive the equations describing the image flow under  $F_3$  expressed in the new variables  $(X, Y, Z)$ . We include them for completeness. They are

$$\dot{X} = Y \quad (6a)$$

$$\dot{Y} = Z \quad (6b)$$

$$\begin{aligned} \dot{Z} &= b\sigma(R-1)X - b(1+\sigma)Y - (1+b+\sigma)Z - X^2Y - \sigma X^3 \\ &\quad + \frac{Y}{X}(Z + (1+\sigma)Y), \end{aligned} \quad (6c)$$

and the parity symmetry is apparent [13,19,20]. Notice the  $1/X$  behavior in the  $\dot{Z}$  equation [13]. The behavior of the vector field as  $X \rightarrow 0$  is direction dependent. In particular, if  $Z = -(1+\sigma)Y$  then the last term in  $\dot{Z}$  vanishes for every  $X$ . Notice that according to Eq. (4)  $X=0$  exactly when  $x=0$ , but then  $Y = \sigma y$  and  $Z = -\sigma(1+\sigma)y$ , or equivalently  $Z = -(1+\sigma)Y$ , which is precisely the condition that the image vector field be well behaved [cf. Equation (6c)].

Before moving on we give the LU-decomposition of  $J_3 = L_3U_3$  which will be useful in the sequel. We have  $U_3 = \text{diag}(1, \sigma, -\sigma x)$  and

$$L_3 = \begin{pmatrix} 1 & 0 & 0 \\ -\sigma & 1 & 0 \\ \sigma(R+\sigma-z) & -1-\sigma & 1 \end{pmatrix}. \quad (7)$$

In this case singularities in  $U_3$  (when  $x=0$ ) correspond to singularities in  $J_3$ .

Now consider the differential mapping  $F_4$  into  $\mathbb{R}^4$ . We will show that this mapping *does* provide an embedding of  $\mathcal{L}$ . The first three coordinates of  $F_4$  are given by  $F_3$  in Eq. (4) and the fourth is given by

$$W = \sigma z(Ax - \sigma y) + \sigma y(B - x^2) - \sigma Cx, \quad (8)$$

where  $A = 1 + b + 2\sigma$ ,  $B = \sigma(R + \sigma + 1) + 1$ , and  $C = R + 2R\sigma + \sigma^2$  are constants depending only on the control parameters. The top  $3 \times 3$  sub-matrix of the Jacobian  $J_4$  is  $J_3$  so that in the LU-decomposition  $J_4 = L_4U_4$ ,  $U_4$  has main diagonal equal to that of  $U_3$  and the top-left  $3 \times 3$  block of  $L_4$  is  $L_3$ . The main diagonal of the rectangular matrix  $U_4$  is the diagonal starting from the upper left entry. The bottom row of  $L_4$  is given by

$$\left[ \sigma Az - \sigma(2xy + C) \quad B - \sigma z - x^2 \quad \sigma \frac{y}{x} - A \quad 1 \right]. \quad (9)$$

It is apparent that  $U_4$  can fail to have maximal rank only if  $x=0$ . However,  $L_4$  contains a term proportional to  $1/x$  and so the rank of  $U_4$  does not indicate the rank of  $J_4$  in this limit. If one first sets  $x=0$  in  $J_4$ , in the new LU-decomposition  $U'_4$  has a main diagonal given by  $\text{diag}(1, \sigma, -\sigma^2y)$  and  $L'_4$  is given by

$$\begin{pmatrix} 1 & 0 & 0 & 0 \\ -\sigma & 1 & 0 & 0 \\ \sigma Az - \sigma C & B - \sigma z & 1 & 0 \\ \sigma(R + \sigma - z) & -(1 + \sigma) & 0 & 1 \end{pmatrix}, \quad (10)$$

which is regular for all  $(x, y, z)$ . Therefore  $F_4$  is singular only along the  $z$  axis, which is disjoint from the Lorenz flow (it is the stable manifold of the central fixed point). We conclude that  $F_4$  provides an embedding of  $\mathcal{L}$  into  $\mathbb{R}^4$ . In fact,  $F_4$  provides an embedding of  $\mathcal{L}$  onto a three dimensional sub-manifold  $M$  of  $\mathbb{R}^4$ . This manifold is disjoint from origin in  $\mathbb{R}^4$ , which is the image of the  $z$ -axis under  $F_4$ . This situation is described further in Sec. V.

The differential mappings  $F_n$  for  $n > 4$  may be analyzed analogously. They all share a similar LU-decomposition such that  $U_n$  has the same main diagonal as  $U_3$  and  $L_n$  possesses a  $1/x$  singularity. Setting  $x=0$  in  $J_n$  gives a  $U'_n$  with main diagonal  $\text{diag}(1, \sigma, -\sigma^2 y)$ , the same as  $U'_4$ , and an  $L'_n$  which is regular on  $\mathbb{R}^3$ , so that the singular set consists of exactly the  $z$  axis in each case. We conclude that the differential mapping  $F_n$  is an embedding into  $\mathbb{R}^n$  for  $n \geq 4$ .

**IV. SYMMETRY**

In this section, we show that the singular sets of the mappings  $F_n$  are symmetry induced, that is, they exist because of the symmetry properties of the original flow and of the chosen observation function. This is not to say that differential mappings for nonsymmetric systems will never possess singularities, but to show that singularities are unavoidable in the present case.

We have seen that the Lorenz system is equivariant under the diffeomorphism  $R_z(\pi): (x, y, z) \mapsto (-x, -y, z)$ . On the other hand, each mapping  $F_n$  is antisymmetric under  $R_z(\pi)$ ,  $F_n(-x, -y, z) = -F_n(x, y, z)$ . We then have the commutative diagram

$$\begin{array}{ccc}
 (x, y, z) & \xrightarrow{F_n} & (X_1, \dots, X_n) \\
 R_z(\pi) \downarrow & & \downarrow P \\
 (-x, -y, z) & \xrightarrow{F_n} & -(X_1, \dots, X_n)
 \end{array} \tag{11}$$

where the map  $P$  is inversion. It follows that each induced flow in  $\mathbb{R}^n$  is parity or  $P$  equivariant. In particular this holds for  $\mathcal{L}_i$  in  $\mathbb{R}^3$ . This change of symmetry is a result of the original system and the observation function together with its derivatives transforming differently under the equivariance group.

The difference of symmetry between the Lorenz flow and the induced flows forces the existence of the singularities in the mappings  $F_n$ , independent of the particular details of how the mappings are constructed. Note that the  $z$  axis is pointwise invariant under  $R_z(\pi)$  while its image is inverted under  $P$ . Equation (11) demands that  $F_n(0, 0, z) = -F_n(0, 0, z)$ , which is only satisfied if the  $z$  axis is mapped to the origin. However, since the  $z$  axis is disjoint from the Lorenz flow this singularity poses no obstruction to obtaining an embedding.

More can be said when  $n=3$ . We will assume that the  $z$  axis is the only singularity of  $F_3$  and show that this leads to a contradiction. Under this assumption  $F_3$  is a diffeomorphism on  $\mathbb{R}^3 - \{z \text{ axis}\}$ . Now the rotation  $R_z(\pi)$  is isotopic (isotopy will be defined in the next section) to the identity through rotations  $R_z(\theta)$  for  $0 \leq \theta \leq \pi$ . It follows that the composition  $F_3 \circ R_z(\theta) \circ F_3^{-1}$  is an isotopy from the map  $P$  to the identity. However,  $P$  is orientation reversing in  $\mathbb{R}^3$  and cannot be isotopic to the identity. Therefore  $F_3$  must have additional singularities. The mildest form this singularity can take is the collapsing of some plane containing the  $z$  axis onto a line (which is parity symmetric).

The preceding argument is no restriction on  $F_n$  for  $n > 3$  since embeddings of  $\mathbb{R}^3$  with different orientation are isotopic in this case [21]. In both of these arguments the essential feature is that the original system is equivariant under an order two symmetry which the observation function is anti-symmetric under. This forces the image system to have a different order two symmetry than the original which in turn forces the existence of singularities. This theme is taken up again in Sec. VII.

**V.  $\mathcal{L}$ ,  $\mathcal{L}_i$ , AND LOCAL REFLECTIONS**

This section specifies how the systems  $\mathcal{L}$  and  $\mathcal{L}_i$  are related in  $\mathbb{R}^3$  and in  $\mathbb{R}^4$ . The mappings  $F_3$  and  $F_4$  seem rather complicated, but their complexity is almost entirely superficial. By allowing smooth deformations the mappings may be brought into simpler forms. Specifically, in  $\mathbb{R}^3$  the two systems differ by a simple mapping called a ‘‘local reflection,’’ which we define below, while in  $\mathbb{R}^4$  the two systems are in fact identical.

The coordinate reflection of  $\mathbb{R}^3$ ,  $(x, y, z) \mapsto (x, y, -z)$  cannot be smoothly deformed in to the identity in  $\mathbb{R}^3$  because it reverses orientation. However, such a smooth deformation is possible in  $\mathbb{R}^4$ . If we consider  $\mathbb{R}^3 \subset \mathbb{R}^4$  as the subspace spanned by the first three coordinates,  $(x, y, z) \mapsto (x, y, z, 0)$ , a deformation (parametrized by  $s$ ) is given by

$$(x, y, z, 0) \rightarrow (x, y, -z \sin s, z \cos s) \rightarrow (x, y, -z, 0), \tag{12}$$

by rotating from  $s = -\pi/2$  to  $\pi/2$ . Notice that this rotation leaves the  $xy$ -plane ( $z=0$ ) pointwise invariant.

From this deformation we can obtain a twisted embedding of  $\mathbb{R}^3$  into  $\mathbb{R}^4$  by allowing the rotation to depend on coordinates of  $\mathbb{R}^3$ . Setting  $s = \arctan x$ , the explicit form of this embedding is then

$$F: (x, y, z) \mapsto \left( x, y, \frac{-xz}{\sqrt{1+x^2}}, \frac{z}{\sqrt{1+x^2}} \right). \tag{13}$$

The projection of this embedding back into  $\mathbb{R}^3$  is singular: it sends the  $yz$ -plane onto the  $y$ -axis. We call this mapping a *local reflection* since it reflects only half of  $\mathbb{R}^3$ . Figure 3 illustrates this phenomenon by demonstrating a twisted embedding of  $\mathbb{R}^2$  into  $\mathbb{R}^3$ . This lower dimensional example may be obtained from Eq. (13) by ignoring the  $y$  coordinate. Any projection of this twisted embedding back into  $\mathbb{R}^2$  results in a singularity.

The denominators in the last two coordinates of Eq. (13) normalize them so that the embedding approaches inclusion as  $x \rightarrow \pm \infty$  (that is, for  $|x|$  large,  $F(x, y, z) \approx (x, y, -z \text{sgn } x, 0)$ , which is the inclusion  $\mathbb{R}^3 \hookrightarrow \mathbb{R}^4$ , at least up to a coordinate reflection).

Through a sequence of deformations, one can show (see Appendix) that the mapping  $F_3$  is equivalent to a local reflection. This relation will be explored further in the following section. In a similar manner one can show that  $F_4$  is equivalent to the standard inclusion  $\mathbb{R}^3 \hookrightarrow \mathbb{R}^4$ . Thus in  $\mathbb{R}^4$  the two systems  $\mathcal{L}$  and  $\mathcal{L}_i$  are the same—one can be smoothly deformed into the other. The systems provide identical *representations* of the Lorenz dynamical system in  $\mathbb{R}^4$  [21]. We

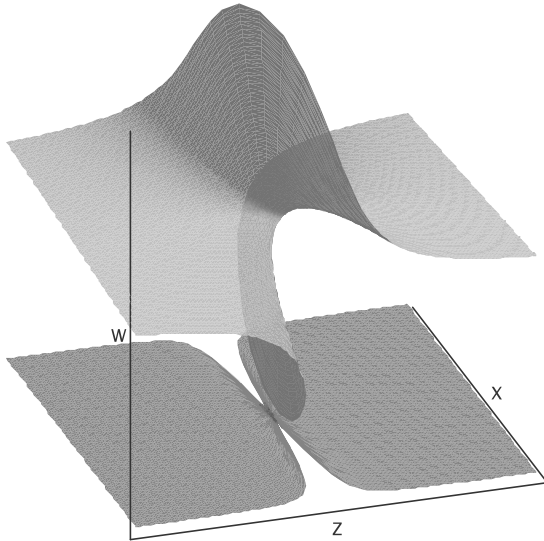


FIG. 3. Twisted embedding of  $\mathbb{R}^2$  in  $\mathbb{R}^3$  and projection onto a local reflection. This is equivalent to the mapping  $F$  in Eq. (13) by ignoring  $y$ .

remark that since the two systems possess different symmetry, the smooth deformation between them cannot be done in a symmetry preserving fashion.

Moreover, we may regard the induced system as providing a three dimensional embedding contained in a three dimensional submanifold  $M \subset \mathbb{R}^4$ . The manifold  $M$  is not  $\mathbb{R}^3$ . Since  $F_4$  is a diffeomorphism away from the  $z$  axis,  $M$  is diffeomorphic to  $\mathbb{R}^3 - \{z\text{-axis}\}$ .

VI.  $\mathcal{L}$ ,  $\mathcal{L}_i$ , AND BRANCHED MANIFOLDS

In the previous section we explored the relationship between the Lorenz and induced Lorenz systems at the level of the differential equations. In this section, we consider how the conclusions of that section apply to the branched manifolds of the two systems, Figs. 1 and 2.

A branched manifold is contained within a handlebody, which is a three-dimensional manifold with boundary. The boundary functions as a trapping surface for the original flow. A handlebody possesses a decomposition into fundamental flow regions called splitting and joining trinions. The branched manifold inside the handlebody has an analogous decomposition into splitting and joining charts. These joining

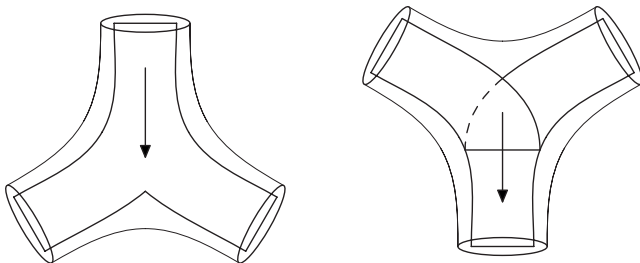


FIG. 4. Trinions with included branched manifold charts: splitting (left) and joining (right). The arrow indicates the flow direction

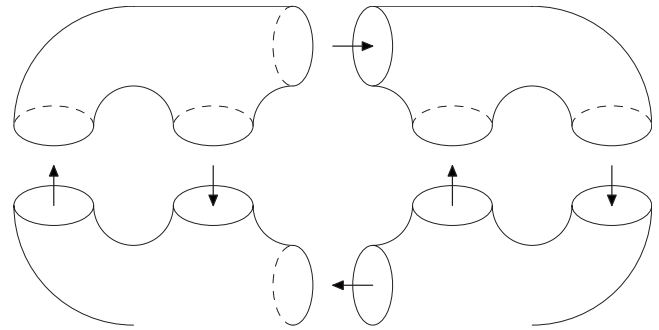


FIG. 5. Genus three handlebody with trinion decomposition. Arrows indicate flow direction between trinions. The branched manifolds of the Lorenz and induced Lorenz systems may be naturally embedded within this handlebody.

and splitting regions are responsible for generating complex dynamical behavior and are shown in Fig. 4.

Both the Lorenz and induced Lorenz systems possess branched manifolds constructed from two joining and two splitting charts. Both systems live inside a genus three handlebody built up from four trinions. The handlebody together with its trinion decomposition is shown in Fig. 5.

A visual inspection of the branched manifolds for  $\mathcal{L}$  (Fig. 1) and  $\mathcal{L}_i$  (Fig. 2) shows that, though they are similar, they differ in two important respects. Both of these differences are in the “bottom” branches that flow from the bottom right trinion to the bottom left one. First, in the Lorenz system this branch twists counter clockwise with respect to the flow direction (cf. Figure 1), while in the induced system it twists clockwise (cf. Figure 2). Second, in the Lorenz system this branch attaches from below while in the induced system it attaches from above. Both of these differences are demanded by the different symmetries of the two systems. The two distinct joining trinions differing in attaching order are shown in Fig. 6.

In Sec. V, we saw that up to isotopy  $\mathcal{L}$  and  $\mathcal{L}_i$  differ by a local reflection of  $\mathbb{R}^3$ . The local reflection collapses vertical lines in the  $yz$ -plane to points along the  $y$  axis. The handlebody carrying  $\mathcal{L}$  intersects the  $yz$  plane twice, once on each side of the  $z$  axis. Each intersection is a disk whose image under the local reflection is a line segment (the disk is collapsed onto a diameter). Therefore, each of these two branches of the handlebody is “pinched” by the local reflection as they pass through the  $yz$  plane. We conclude that in  $\mathbb{R}^3$  the natural handlebody containing  $\mathcal{L}_i$  is *not* the image of

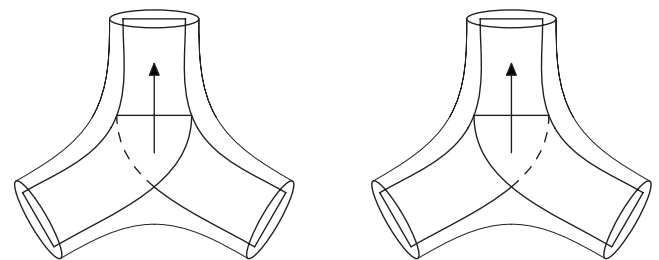


FIG. 6. The two types of joining trinion related by a reflection in the  $z$  direction (out of the page). The top exit branch is a subset of the  $xy$  plane, which is invariant under reflections

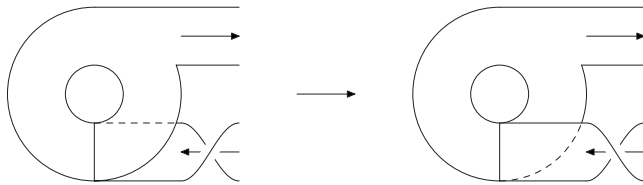


FIG. 7. Effect of the change of orientation  $z \rightarrow -z$  (out of the page) induced by the local reflection on half of the Lorenz branched manifold. Arrows indicate the flow direction.

the handlebody containing  $\mathcal{L}$ . This is a reflection of the fact established in Sec. III that  $F_3$  is not a diffeomorphism on any neighborhood of the attractor and therefore does not represent the entire Lorenz flow. The image handlebody is, however, well defined in  $\mathbb{R}^4$  but has a singular projection in  $\mathbb{R}^3$ .

Next, consider the effect of the local reflection on the Lorenz branched manifold. The two horizontal branches that run through the horizontal tubes of the handlebody each cut the  $yz$  plane in a horizontal line segment. However, this line segment is *invariant* under the action of the local reflection; no two points are identified. Recall that the local reflection preserves the orientation of  $\mathbb{R}^3$  on one side of the singular set and reverses it on the other by sending  $z \rightarrow -z$ . The effect of this reversal on half of the branched manifold is shown in Fig. 7 [13]. This is precisely the operation that takes the Lorenz branched manifold onto the induced Lorenz branched manifold.

In general, if a dynamical system and its image under some mapping into  $\mathbb{R}^3$  have branched manifolds that are the same except for a pair of joining charts that are of opposite type the mapping cannot be a diffeomorphism of the flow. The two joining charts are related by a reflection, but the other charts are related without reflection, so a local reflection is required somewhere for the corresponding handlebody and trinions to match up correctly. Since a local reflection is the singular projected image into  $\mathbb{R}^3$  of a smooth embedding into  $\mathbb{R}^4$ , there is no distinction between the two joining trinions in  $\mathbb{R}^4$ .

Finally, that the two branched manifolds are diffeomorphic can also be seen by considering the mapping  $F_3$ . Recall that the singularity along the  $yz$ -plane collapses the lines  $y = \text{const}$ . By applying the Birman-Williams projection on the Lorenz flow one obtains a branched two-manifold that cuts the  $yz$  plane transversely in the form of a graph over  $y$  (see Fig. 8). Therefore, no two points of the branched manifolds are identified by  $F_3$  and the Birman-Williams projection commutes with this mapping and the two branched manifolds are diffeomorphic.

Several previous studies have been carried out to determine how many inequivalent representations can be constructed for three-dimensional dynamical systems, or more specifically their strange attractors [21–23]. In [22] it was shown that if the attractor was contained in a genus-one bounding torus, its inequivalent representations differed by global torsion, parity, and knot type. In [23] it was found that, neglecting knot type, inequivalent representations (or embeddings) differ by local rotation and local reflection operations. A local rotation is obtained by inserting a tube at each output port in a trinion decomposition of a genus- $g$

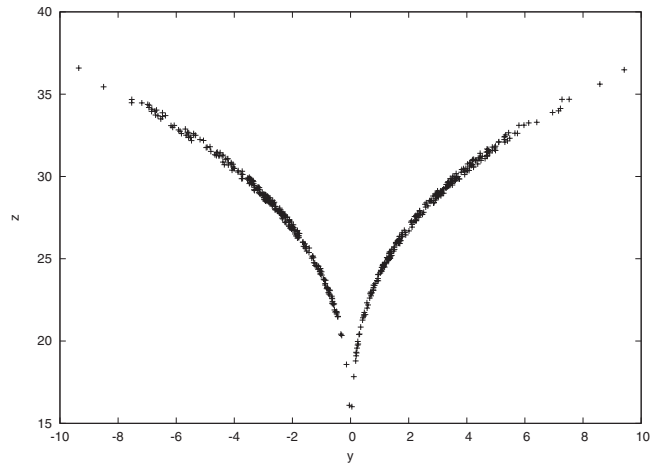


FIG. 8. Intersection of the Lorenz flow with the  $yz$  plane. The fuzziness of this intersection is in the stable direction of the flow. Since the Birman-Williams projection collapses orbits along the stable direction the fuzziness disappears, resulting in a set describable as a graph over  $y$ .

handlebody and allowing the flow through that tube to be rotated through an integer number of  $2\pi$  radians. In this way it is possible to associate an integer index to each such flow tube, of which there are  $3(g-1)$  for a genus- $g$  handlebody. A local reflection has the form shown in Fig. 7. There are  $g-1$  regions in the decomposition of a genus- $g$  handlebody that can be subjected to local reflections. Local reflections in genus- $g$  handlebodies are subject to all the restrictions discussed above. The present manuscript clarifies that local reflections are the result of projections of local rotations from higher dimensional embeddings. In three dimensions local reflections describe embeddings of the branched manifold, not the flow whose projection is the branched manifold. In order to construct embeddings for the flow, the mapping must be into one higher dimension [21].

### VII. $R_z(\pi)$ EQUIVARIANT EMBEDDINGS

It has been observed [3] that one cannot obtain a rotationally equivariant embedding of the Lorenz system from a differential embedding based on a single observable. It is the purpose of this section to demonstrate this explicitly. More generally, we show that if a differential embedding of a dynamical system with an order two symmetry possesses symmetry, it is necessarily parity symmetry. Of course, embeddings with the same symmetry do exist (e.g., the identity map), therefore such embeddings cannot be constructed through successive derivatives of any observation function, that is, they are not differential embeddings in the usual sense.

Suppose that a dynamical system  $\dot{x}=v(x)$  is equivariant under a mapping (group operation)  $g$ , so that  $v(gx)=gv(x)$ . Let  $f$  be an eigenfunction of  $g$  satisfying  $f(gx)=\pm f(x)$ . This is equivalent to saying that  $f$  has definite parity (either even or odd) under  $g$ . We show that if  $f$  is an eigenfunction then  $d/dt|_0 f(\varphi_t(x))$  is an eigenfunction of the same parity, where  $\varphi_t$  is the flow associated to  $v$ .

By definition of derivative

$$\frac{d}{dt} \Big|_0 f[\varphi_t(x)] = \lim_{t \rightarrow 0} \frac{f[\varphi_t(x)] - f(x)}{t} = \lim_{t \rightarrow 0} \frac{f(x + tv_x) - f(x)}{t}. \tag{14}$$

Now by transforming  $x \mapsto gx$  we have

$$\begin{aligned} \frac{d}{dt} \Big|_0 f[\varphi_t(gx)] &= \lim_{t \rightarrow 0} \frac{f(gx + tv_{gx}) - f(gx)}{t} \\ &= \lim_{t \rightarrow 0} \frac{f[g(x + tv_x)] - f(gx)}{t} \\ &= \frac{d}{dt} \Big|_0 f\{g[\varphi_t(x)]\}, \end{aligned} \tag{15}$$

where in the second line we used the assumption of equivariance. It is now apparent that this expression is an eigenfunction of the same parity as  $f$  under  $g$ . By induction the higher derivatives are eigenfunctions of the same parity. Now a differential mapping  $F_n$  constructed from  $f$  is given by  $F_n = (f_1, f_2, \dots, f_n)$ . Here,  $f_1 \equiv f$  and for  $i > 1$   $f_i$  is the time derivative of  $f_{i-1}$ . It follows that when  $f$  has definite parity that  $F_n$  has the same definite parity.

Therefore if  $f$  is odd under  $g$  then the corresponding differential mapping  $F_n$  will be odd and the image system will be parity equivariant. If on the other hand  $f$  is even then the differential mapping  $F_n$  will be even and thus necessarily two-to-one since  $F_n(x) = F_n(gx)$ . The image is therefore trivially equivariant or invariant. For example,  $z$  is even, and a differential mapping based on  $z$  yields a two-to-one mapping onto the proto-Lorenz system. Explicit equations may be found in [20].

Now let  $f$  be any observation function and make an eigen-decomposition of  $f$  as  $f = f^+ + f^-$ , where  $f^\pm$  are the even (+) and odd (-) parts of  $f$  under  $g$ . Since the derivative is linear, the components  $f_i$  of the differential mapping  $F_n$  split into even and odd parts  $f_i^\pm$ , which are just the even and odd parts of  $i$ th derivative of  $f$ .

Now suppose that  $g = R_z(\pi)$ . We show that equivariance of the image under  $g$  leads to a contradiction. In order for the image to be  $g$  equivariant  $F_3$  must be  $g$  equivariant. Suppose first that the principal directions of  $g$  align with the components of  $F_3$ . Since up to a permutation of the axes  $g = \text{diag}(-1, -1, 1)$ , every component function  $f_i$  must be an eigenfunction, two with eigenvalue  $-1$  (odd) and one with eigenvalue  $+1$  (even). In any case the component  $f_1 = f$  is an eigenfunction, but we have seen that its derivatives are necessarily eigenfunctions of the same parity which yields a contradiction. Thus  $F_3$  cannot be equivariant under  $g$ .

More generally, suppose that  $y_i$  are equivariant coordinates linearly related to the  $f_j$  by  $y_i = M_i^j f_j$ . Assume without loss of generality that  $y_1$  is even. Then we must have  $M_1^j f_j^- = 0$ , which says that the  $f_j^-$  are linearly dependent. In the same way  $y_2$  and  $y_3$  being odd force the  $f_j^+$  to be linearly dependent. Therefore all  $f_j$  are linearly dependent, but then  $F_3$  cannot be an embedding. We therefore conclude that no

differential embedding of a  $R_z(\pi)$  equivariant dynamical system can be  $R_z(\pi)$  equivariant, the Lorenz system in particular.

The general case follows at once. The generator of any order two symmetry acting in  $\mathbb{R}^n$  is given in the appropriate basis by  $g = \text{diag}(\pm 1, \pm 1, \dots, \pm 1)$ , where the signs are incoherent, and we have  $g^2 = I_n$ . The previous considerations show a differential embedding will not be equivariant under  $g$ , but rather  $I_n$  or  $-I_n$ . In the first case the image is invariant, and in the second case it is parity equivariant. However, as we have seen, it is possible for a system and its parity equivariant image to be diffeomorphic, even isotopic.

Finally, we note that in the spirit of [2], a pair of observation functions, one even under  $g$  and the other odd, may be used to reconstruct any order-two symmetry. In particular, the projection of a generic (nonsymmetric) measurement function  $f$  onto the even ( $f_+$ ) and odd ( $f_-$ ) eigendirections suffices. For the Lorenz system,  $f = x + z$  has the projections  $f_+ = z$  and  $f_- = x$ . These projections are mapped into the two dimensional space of embedding parameters  $f \rightarrow (f_-, f_+) \in V = \mathbb{R}^2$  as described in [2]. For the Lorenz system, the mapping of generic data into  $V^4 = V + \dot{V} + \ddot{V} + \dots \in \ddot{V} = \mathbb{R}^8$  produces a three-dimensional manifold with  $Z_2$  symmetry

$$(+ +, + +, + +, + +) \xrightarrow{g} (- +, - +, - +, - +).$$

Projections into three-dimensional subspaces with  $n_o$  odd directions and  $n_e$  even directions results in attractors in  $\mathbb{R}^3$  with inversion symmetry ( $n_o = 3, n_e = 0$ ), rotation symmetry (2,1), reflection symmetry (1,2), and no symmetry (0,3). These projections may not be embeddings; failure to be an embedding is due entirely to the projection [24]. The last projection cannot be an embedding because it is two to one.

### VIII. CONCLUSIONS

We have analyzed differential mappings of the rotationally equivariant Lorenz dynamical system  $\mathcal{L}$  in some detail. While the mapping constructed from the  $x$  coordinate and its first two derivatives is one-to-one on the attractor of  $\mathcal{L}$ , it does not provide a diffeomorphism of the flow. The induced Lorenz system  $\mathcal{L}_i$  is not diffeomorphic to the Lorenz system in  $\mathbb{R}^3$ . However, the differential mappings of  $\mathcal{L}$  into  $\mathbb{R}^n$  for  $n \geq 4$  do yield embeddings. We saw that the failure to achieve an embedding in  $\mathbb{R}^3$  was related to the different symmetry properties of  $\mathcal{L}$  and  $\mathcal{L}_i$ : the former is rotationally equivariant and the latter is parity equivariant. We then showed that the two systems are actually isotopic in  $\mathbb{R}^4$  and showed how their associated bounding tori and branched manifolds are related. Finally, we worked out the details of the observation made in [3] that no differential mapping of the Lorenz system is rotationally equivariant; any equivariant image of such a system is either invariant, possessing no nontrivial symmetry, or else is parity equivariant with a twofold symmetry. We then generalized this result to show that an equivariant reconstruction of any system with a twofold symmetry is parity symmetric. Finally, we showed how to recover an arbitrary twofold symmetry from a generic observation function.

While it is not possible to embed the Lorenz system into the three dimensional manifold  $\mathbb{R}^3$  it is possible to embed it into a three-dimensional twisted submanifold  $M$  of  $\mathbb{R}^4$ . The projection of this manifold into  $\mathbb{R}^3$  possesses singularities. In particular, the projection induces a local reflection.

#### ACKNOWLEDGMENT

We thank C. Letellier for useful discussions.

#### APPENDIX: MAPPING DEFORMATIONS

The purpose of this appendix is to fill in the technical details of Sec. V by constructing explicit deformations of the mappings  $F_3$  and  $F_4$  to a local reflection and inclusion respectively. The idea of a smooth deformation of an embedding is made precise through the notion of *isotopy*. Two embeddings  $f$  and  $g$  are isotopic if there is a smooth map  $h(x, s)$ ,  $s \in [0, 1]$ , that satisfies the following three properties: 1) for every fixed  $s$ ,  $h_s(x) \equiv h(x, s)$  is an embedding; 2)  $h_0 = f$ ; and 3)  $h_1 = g$ . We will refer to either  $h(x, s)$  or  $h_s(x)$  as the isotopy. Thinking of  $s$  as time, the isotopy smoothly transforms the embedding  $f$  at time zero to the embedding  $g$  at time one through a sequence of embeddings. It is natural to regard isotopic embedding's as the same or equivalent. We note that it will often be convenient to define an isotopy over an interval other than  $[0, 1]$ . In all cases the isotopies defined will be obviously smooth, so one need only check that they are one-to-one for each  $s$ .

Recall the twisted embedding Eq. (13), and the denominators of the last two coordinate which normalized them to approach inclusion as  $|x| \rightarrow \infty$ . This embedding is isotopic to the un-normalized mapping

$$G:(x, y, z) \mapsto (x, y, -xz, z). \quad (16)$$

One can take for the deformation  $(1-s)F + sG$  with  $s \in [0, 1]$  and check that this is one-to-one for each  $s$ . We may also refer to the first three coordinates of this mapping as a local reflection of  $\mathbb{R}^3$ .

The mapping  $F_3$  defines a rather complicated embedding of  $\mathbb{R}^3 - \{yz\text{-plane}\}$  into  $\mathbb{R}^3$ . Denote the image of  $(x, y, z)$  by  $(X, Y, Z) = F_3(x, y, z)$  and recall that these coordinates are given by Eq. (4). We will now simplify  $F_3$  through a sequence of isotopies. We note that the isotopies need only be

one-to-one away from the  $yz$ -plane since  $F_3$  is singular there. In each case  $s \in [0, 1]$ . Our goal is to show that  $F_3$  is isotopic to a local reflection.

First note that the first coordinate is already  $X=x$ . Next, by smoothly rescaling the axes, the overall factor of  $\sigma$  on the last two components may be set to one. The second coordinate is now given by  $Y=y-x$ . By defining  $Y_s = y + (s-1)x$  this coordinate can be smoothly changed to  $Y=y$ . One can check that this is one-to-one for every  $s$ . For the third coordinate define  $Z_s = Z(1-s) - szx$  to smoothly deform it to  $-zx$ . In this case points with different  $z$  coordinate are identified when  $x=0$ . In fact, when  $x=0$ ,  $Z_s = (s-1)(1+\sigma)y$ , so for every  $s$  the  $yz$  plane is taken to a line. The form of the singularity is preserved during this deformation and  $Z_s$  defines an isotopy of  $F_3$  away from its singular set. We have thus succeeded in bring  $F_3$  to the form of (the first three coordinates of) Eq. (16) through a sequence of deformations. This proves the claim in Sec. V that the attractors  $\mathcal{L}_i$  and  $\mathcal{L}$  differ by a local reflection in  $\mathbb{R}^3$ .

Now we consider the embedding  $F_4$  into  $\mathbb{R}^4$ . Since the first three coordinate of  $F_4$  are given by  $F_3$ , the above isotopies apply to  $F_4$  as well. However, the isotopy  $Z_t$  was singular for  $F_3$  along  $x=0$ . By checking the fourth coordinate  $W$  of  $F_4$  given in Eq. (8) we see that points are identified only when  $y=0$  as well. But this defines the  $z$  axis, which is the singular set of  $F_4$ . We conclude that  $Z_t$  is an isotopy away from the singular set of  $F_4$ .

It remains only to transform the final coordinate  $W$  to  $z$  to arrive at the twisted embedding Eq. (16). This can be done through a sequence of deformations,  $W \rightarrow z(x-y) \rightarrow zx \rightarrow z$ . At each step the deformation is linear:  $f \rightarrow g$  by  $sg + (1-s)f$ . It is tedious but straightforward to check that each deformation is one-to-one away from the  $z$  axis and so completes the isotopy of  $F_4$  to the twisted embedding. Finally, the twisted embedding is isotopic to the standard inclusion  $\mathbb{R}^3 \hookrightarrow \mathbb{R}^4$ . This can be achieved by the isotopy

$$(x, y, z, s) \rightarrow (x, y, -z \sin \xi, z \cos \xi), \quad (17)$$

where we set

$$\xi = s \arctan x + (s-1)\pi/2, \quad (18)$$

and  $s \in [0, 1]$ . We conclude that  $F_4$  is isotopic to the inclusion  $\mathbb{R}^3 \hookrightarrow \mathbb{R}^4$ . This proves the claim in Sec. V that the attractors  $\mathcal{L}_i$  and  $\mathcal{L}$  are identical in  $\mathbb{R}^4$ .

- 
- [1] F. Takens, in *Dynamical Systems and Turbulence*, edited by D. A. Rand and L. S. Young, Lecture Notes in Mathematics (Springer-Verlag, New York, 1981), Vol. 898, pp. 366–381.
- [2] G. P. King and I. Stewart, *Physica D* **58**, 216 (1992).
- [3] C. Letellier and G. Gouesbet, *J. Phys. II France* **6**, 1615 (1996).
- [4] D. J. Cross and R. Gilmore (unpublished).
- [5] G. B. Mindlin, H. G. Solari, M. A. Natiello, R. Gilmore, and X.-J. Hou, *J. Nonlinear Sci.* **1**, 147 (1991).
- [6] R. Gilmore, *Rev. Mod. Phys.* **70**, 1455 (1998).
- [7] R. Gilmore and M. Lefranc, *The Topology of Chaos: Alice in Stretch and Squeezeland* (Wiley, New York, 2002).
- [8] W. H. Press, S. A. Teukolsky, W. T. Vetterling, and B. P. Flannery, *Numerical Recipes in C*, 2nd ed. (Cambridge University Press, New York, 1992).
- [9] C. Letellier, L. A. Aguirre, and U. S. Freitas, *Chaos* **19**, 023103 (2009).
- [10] J. S. Birman and R. F. Williams, *Topology* **22**, 47 (1983).
- [11] J. S. Birman and R. F. Williams, *Contemp. Math.* **20**, 1 (1983).
- [12] C. Letellier and R. Gilmore, *Phys. Rev. E* **63**, 016206 (2000).

- [13] R. Gilmore and C. Letellier, *The Symmetry of Chaos* (Oxford University Press, New York, 2007).
- [14] T. D. Sauer, *Scholarpedia J.* **1**, 1727 (2006).
- [15] C. Letellier and L. A. Aguirre, *Chaos* **12**, 549 (2002).
- [16] C. Letellier, L. A. Aguirre, and J. Maquet, *Phys. Rev. E* **71**, 066213 (2005).
- [17] C. Letellier and L. A. Aguirre, *Phys. Rev. E* **72**, 056202 (2005).
- [18] C. Letellier and L. A. Aguirre, *Phys. Rev. E* **79**, 066210 (2009).
- [19] G. Gouesbet, *Phys. Rev. A* **46**, 1784 (1992).
- [20] G. Gouesbet and C. Letellier, *Phys. Rev. E* **49**, 4955 (1994).
- [21] D. J. Cross and R. Gilmore, *Phys. Rev. E* **80**, 056207 (2009).
- [22] N. Romanazzi, M. Lefranc, and R. Gilmore, *Phys. Rev. E* **75**, 066214 (2007).
- [23] R. Gilmore, C. Letellier, and N. Romanazzi, *J. Phys. A: Math. Theor.* **40**, 13291 (2007).
- [24] T. Poston and I. Stewart, *Catastrophe Theory and its Applications* (Dover, New York, 1996).